

# Fast Safe Rectangular Corridor-based Online AGV Trajectory Optimization with Obstacle Avoidance

Shaoqiang Liang<sup>1</sup>, Songyuan Fa<sup>1</sup>, Zong Chen<sup>1</sup> and Yiqun Li<sup>1</sup>

**Abstract**—Automated Guided Vehicles (AGVs) are widely adopted in various industries due to their efficiency and adaptability. However, safely deploying AGVs in dynamic environments remains a significant challenge. This paper introduces an online trajectory optimization framework, the Fast Safe Rectangular Corridor (FSRC), designed for AGVs in obstacle-rich settings. The primary challenge is efficiently planning trajectories that prioritize safety and collision avoidance. To tackle this challenge, the FSRC algorithm constructs convex regions, represented as rectangular corridors, to address obstacle avoidance constraints within an optimal control problem. This conversion from non-convex to box constraints improves the collision avoidance efficiency and quality. Additionally, the Modified Visibility Graph algorithm speeds up path planning, and a boundary discretization strategy expedites FSRC construction. The framework also includes a dynamic obstacle avoidance strategy for real-time adaptability. Our framework’s effectiveness and superiority have been demonstrated in experiments, particularly in computational efficiency (see Fig. 6 and 7). Compared to state-of-the-art frameworks, our trajectory planning framework significantly enhances computational efficiency, ranging from 1 to 2 orders of magnitude (see Table II). Notably, the FSRC algorithm outperforms other safe convex corridor-based methods, substantially improving computational efficiency by 1 to 2 orders of magnitude (see Table III).

## I. INTRODUCTION

Recently, the deployment of Automated Guided Vehicles (AGVs) has witnessed a significant upsurge across diverse industrial and logistical contexts [1]. Their growing popularity can be attributed to their efficiency and adaptability [2], finding applications in sectors such as mining [3], surveillance [4], forklift operations [5], traffic management [6], electronic manufacturing [7], and IoT scenarios [8]. AGVs promise to automate warehouse operations, curb operational costs, and enhance overall production processes [9], [10]. However, effectively and safely employing AGVs in dynamic environments [11], [12], such as smart factories and IoT-enabled locations [13], remains a formidable challenge.

In AGV systems’ core, trajectory planning optimization assume pivotal roles. As AGVs traverse intricate and ever-evolving environments, the paramount task is to navigate expertly while avoiding collisions with stationary and moving obstacles. The exigencies of real-time AGV operations underscore the critical role played by efficient trajectory

This research was funded by the National Natural Science Foundation of China (Grant No. 51905185) and the National Postdoctoral Program for Innovative Talents No. BX20180109. (Corresponding author: Yiqun Li).

<sup>1</sup>Shaoqiang Liang, Songyuan Fa, Zong Chen, and Yiqun Li are affiliated with the State Key Laboratory of Intelligent Manufacturing Equipment and Technology, School of Mechanical Science and Engineering, Huazhong University of Science and Technology, Wuhan 430074, China. sqliang@hust.edu.cn, liyiqun@hust.edu.cn

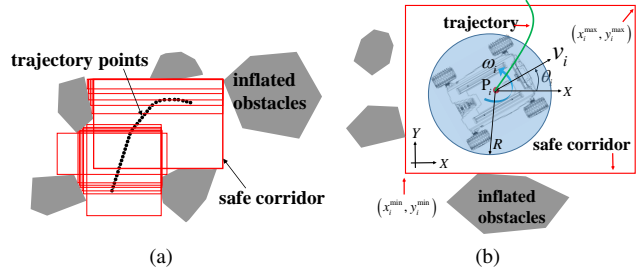


Fig. 1: (a) Safe convex corridor-based methods, (b) The kinematic model of the AGV.

planning algorithms. These algorithms are indispensable for swiftly adapting to changing situations, ensuring safety, and minimizing travel time. Nevertheless, classical algorithms such as RRT [14], RRT\* [15], A\* [16], hybrid A\* [17], adaptive state lattices [18], [19], and deep reinforcement learning-based methods [20]–[22] often fall short in meeting these rigorous requirements. Consequently, they yield trajectories of suboptimal quality, necessitating subsequent optimization.

In contrast, optimization-based methods approach the problem as an optimal control problem (OCP) and employ numerical techniques to derive trajectories [23]–[25]. However, the obstacle avoidance constraints in OCP are typically non-convex, which can lead to slow solving speeds, especially in complex scenarios. To address this issue, safe convex corridor-based methods [26]–[30] confine AGVs to move within corresponding convex regions, as visualized by the rectangular boxes in Fig. 1a. The AGV’s path points must remain within these rectangular boxes, ensuring collision-free and safe navigation. This transformation effectively converts non-convex obstacle avoidance constraints into linear constraints, significantly improving the efficiency and quality of OCP solving [26], [27], [30]. Nevertheless, it is imperative to emphasize that generating these convex regions should not unduly consume time, as it has the potential to impact the real-time nature of the trajectory planning module.

Moreover, the efficiency of optimization-based methods is impacted by the quality of the initial solution [31]. Therefore, employing path planning algorithms is imperative to furnish an initial solution, which is also relied upon by safe convex corridor methods to establish a safe corridor. Nonetheless, the search speeds of algorithms like A\* and hybrid A\* are constrained by map size and precision, while RRT and RRT\* exhibit instability and do not guarantee the shortest path.

Taking all factors into account, we present a fast trajectory planning framework based on the Fast Safe Rectangular Corridor (FSRC). The key contributions are as follows:

- 1) The FSRC algorithm is introduced, significantly accelerating the process of constructing convex regions compared to STC [26] and SFC [26]. The corridors established by FSRC serve as representations for obstacle avoidance constraints within OCP, effectively eliminating redundant obstacle constraints from the surrounding environment.
- 2) The Modified Visibility Graph (MVG) is proposed, demonstrating remarkable path-searching speeds.
- 3) A boundary discretization strategy is introduced, substantially improving the construction speed of FRSC.
- 4) A dynamic obstacle avoidance strategy is presented, enabling real-time obstacle avoidance for AGVs.

The remainder of this paper is organized as follows: Section 2 establishes the discrete trajectory planning problem. Section 3 details the specific implementation algorithms of the trajectory planning framework, including obstacle inflation and discretization, the MVG, the FRSC, and the dynamic obstacle avoidance strategy. Section 4 provides experimental results, and Section 5 concludes the paper.

## II. PROBLEM FORMULATION

Our objective is to perform real-time trajectory planning and obstacle avoidance for AGVs, presenting a discrete trajectory planning problem below aimed at minimizing time.

$$\text{Minimize } J = T_f - T_0 \quad (1a)$$

Subject to

$$x_{i+1} - x_i = v_i \cdot \cos \theta_i \cdot \Delta_t, \quad 1 \leq i \leq N-1 \quad (1b)$$

$$y_{i+1} - y_i = v_i \cdot \sin \theta_i \cdot \Delta_t, \quad 1 \leq i \leq N-1 \quad (1c)$$

$$v_{i+1} - v_i = a_i \cdot \Delta_t, \quad 1 \leq i \leq N-1 \quad (1d)$$

$$\theta_{i+1} - \theta_i = \omega_i \cdot \Delta_t, \quad 1 \leq i \leq N-1 \quad (1e)$$

$$x_1 = x_{T_0}, \quad y_1 = y_{T_0}, \quad \theta_1 = \theta_{T_0} \quad (1f)$$

$$v_1 = v_{T_0}, \quad a_1 = a_{T_0}, \quad \omega_1 = \omega_{T_0} \quad (1g)$$

$$x_N = x_{T_f}, \quad y_N = y_{T_f} \quad (1h)$$

$$v_N = v_{T_f}, \quad a_N = a_{T_f}, \quad \omega_N = \omega_{T_f} \quad (1i)$$

$$x_i^{\min} \leq x_i \leq x_i^{\max}, \quad y_i^{\min} \leq y_i \leq y_i^{\max}, \quad 1 \leq i \leq N \quad (1j)$$

$$v_i^{\min} \leq v_i \leq v_i^{\max}, \quad a_i^{\min} \leq a_i \leq a_i^{\max}, \quad 1 \leq i \leq N \quad (1k)$$

$$\omega_i^{\min} \leq \omega_i \leq \omega_i^{\max}, \quad 1 \leq i \leq N \quad (1l) \quad (1)$$

where  $T_0$  and  $T_f$  denote the starting and ending times, discretized into  $N - 1$  segments via the forward Euler method [32]. Equations (1b-1e) capture kinematic constraints for omnidirectional movement.  $P_i(x_i, y_i)$  signifies geometric center (see Fig. 1b), while  $v_i$ ,  $a_i$ ,  $\omega_i$ , and  $\theta_i$  represent velocity, acceleration, angular velocity, and yaw angle at  $P_i$ . (1f-1i) define the boundary constraints for the AGV's starting and ending poses. (1j) represent the obstacle avoidance constraint implemented by FSRC. (1k) and (1l) limit the AGV's velocity, acceleration, and angular velocity. (1b) and (1c) being nonlinear constraints, they are converted into soft

constraints, resulting in a modified objective function:

$$\begin{aligned} J = & (T_f - T_0) + \varpi_1 \sum_{i=1}^{N-1} (x_{i+1} - x_i - v_i \cdot \cos \theta_i \cdot \Delta_t)^2 \\ & + \varpi_2 \sum_{i=1}^{N-1} (y_{i+1} - y_i - v_i \cdot \sin \theta_i \cdot \Delta_t)^2 \end{aligned} \quad (2)$$

Here,  $\varpi_1$  and  $\varpi_2$  represent penalty function weights.

## III. ALGORITHM

This section introduces obstacle handling, MVG for path planning, FRSC, and dynamic obstacle avoidance strategy.

### A. Obstacle Inflation and Discretization

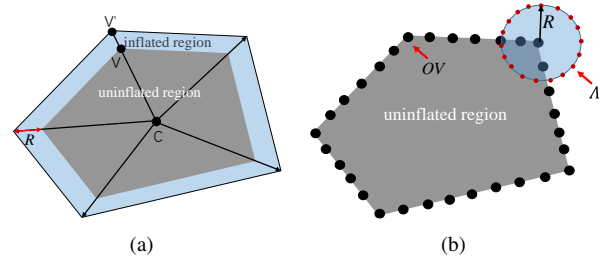


Fig. 2: Inflation of Obstacles and discretization

Before the path planning, essential tasks involving obstacle inflation and discretization take place. These tasks encompass the gathering of three crucial sets: the expanded polygonal obstacle edges set  $\Xi$  and inflated obstacle vertex set  $\Psi$ , utilized for obstacle avoidance of MVG, and the inflation obstacle node set  $\Lambda$ , used to establish a safe rectangular corridor. These procedures are comprehensively depicted in Algorithm 1. Here,  $R$  represents the coverage circle radius of the AGV (see Fig. 1b),  $N_{obs}$  denotes the number of obstacles,  $C_i$  represents the geometric center of obstacle  $i$ , and  $(ox_{ij}, oy_{ij})$  denote the vertices of the obstacle. Fig. 2 illustrates the process of obstacle inflation and discretization, Fig. 2a demonstrates the acquisition of  $\Xi$ , and Fig. 2b illustrates the acquisition of  $\Lambda$ .

---

#### Algorithm 1 Obstacle handling

**Require:** obstacles  $O$ , radius  $R$ , discretization precision  $\ell$

- 1:  $\Xi \leftarrow \emptyset$ ,  $\Lambda \leftarrow \emptyset$ ,  $OV \leftarrow \emptyset$ ,  $\Psi \leftarrow \emptyset$ ,
- 2: **for**  $i \leftarrow 1$  to  $N_{obs}$  **do**
- 3:    $C_i \leftarrow \left( \sum_{j=1}^{N_{V_i}} ox_{ij}, \sum_{j=1}^{N_{V_i}} oy_{ij} \right) / N_{V_i}$
- 4:   **for**  $j \leftarrow 1$  to  $N_{V_i}$  **do**
- 5:      $V'_{ij} \leftarrow \text{expand}(R, V_{ij})$  in the direction  $\overrightarrow{C_i V_{ij}}$
- 6:     add  $V'_{ij} \leftarrow$  to  $\Psi$
- 7:     add  $[V'_{i,0}, V'_{i,N_{V_i}}]$  to  $\Xi$
- 8:   **for**  $j \leftarrow 1$  to  $N_{V_i} - 1$  **do**
- 9:     add  $[V'_{i,j}, V'_{i,j+1}]$  to  $\Xi$
- 10: **end for**
- 11:  $OV \leftarrow \text{discretizeBoundary}(O_i, \ell)$
- 12:  $\Lambda_i \leftarrow \text{inflateBoundary}(OV, R, \ell)$
- 13: add  $\Lambda_i$  to  $\Lambda$
- 14: **return**  $\Lambda, \Xi$  and  $\Psi$

---

### B. Modified Visibility Graph

Building upon [33], the Modified Visibility Graph (MVG) algorithm for path planning is introduced, as depicted in Algorithm 2. This approach encompasses three primary phases. Firstly, a bidirectional weighted graph  $G$  is created using the start point  $s$ , the goal point  $g$ , the expanded polygonal obstacle edges  $\Xi$ , and the inflated obstacle vertex set  $\Psi$ . A compact adjacency list  $\mathcal{L}$  is employed to efficiently represent this graph  $G$ . The weights between nodes are distance-based, and infinite values indicate collisions. Collision-free paths are delineated by line segments that do not intersect any line segment within  $\Xi$ . Secondly, the Dijkstra search [34] focuses on finding the shortest path between  $s$  and  $g$  rather than examining all possible node pairs. The search concludes once the shortest path between  $s$  and  $g$  is identified. Thirdly, the outcomes of the second phase are uniformly discretized into  $N$  path points. The example can be referenced in Fig. 3.

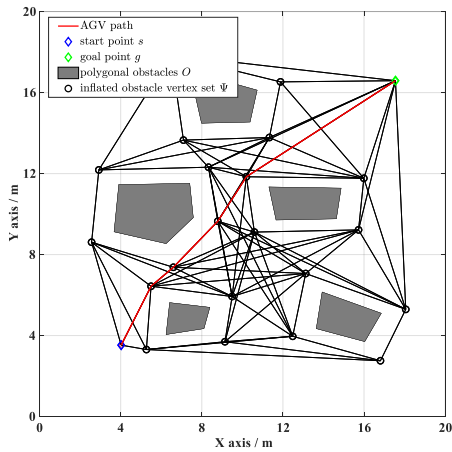


Fig. 3: Results of the Modified Visibility Graph.

#### Algorithm 2 Modified Visibility Graph (MVG)

**Require:** start point  $s$ , goal point  $g$ ,  $\Xi$ ,  $\Psi$ , number of path points  $N$

- 1:  $\mathcal{L} \leftarrow \text{constructAdjacencyList} (s, g, \Xi, \Psi)$
- 2:  $(pX, pY) \leftarrow \text{Dijkstra} (\mathcal{L}, s, g)$
- 3:  $\text{path} \leftarrow \text{discretePath} (pX, pY, N)$
- 4: **return**  $\text{path}$

### C. Fast Safe Rectangular Corridor

In this section, we introduce the concept of a rectangular bounding box denoted as  $\mathcal{B}_{\mathcal{R}}(i, :)$ , corresponding to each path point  $P_i$ . In the Problem (1), ensuring that  $P_i$  falls within its corresponding bounding box,  $\mathcal{B}_{\mathcal{R}}(i, :)$ , is established as constraint (1j). To achieve this constraint, we present the Fast Safe Rectangular Corridor (FSRC) algorithm, outlined in Algorithm 3, which streamlines the creation of these rectangular boxes. Below, we delve into the step-by-step process of constructing  $\mathcal{B}_{\mathcal{R}}$ .

To begin, the bounding boxes of two adjacent path points often exhibit overlapping tendencies owing to their proxim-

ity. To avoid redundant box creation, a check is conducted: if  $P_i$  is within the boundaries of the preceding bounding box,  $\mathcal{B}_{\mathcal{R}}(i - 1, :)$ , the current process is skipped. This omission step can be repeated up to a maximum of  $T_m$  times.

Moving forward, we initiate a bounding box denoted as  $\mathcal{B}_{\mathcal{R}}(i, :)$  with dimensions of  $2L_m \times 2L_m$ . To identify the set of remaining obstacle nodes, represented as  $\Lambda_{\mathcal{R}}$ , we exclude nodes that fall outside the confines of  $\mathcal{B}_{\mathcal{R}}(i, :)$ . This operation is carried out via the `obsCheck()` function. When  $\Lambda_{\mathcal{R}}$  is empty, it signifies the absence of obstacles within the current bounding box, allowing us to skip subsequent steps. Furthermore, we ensure that any subsequent expansion does not exceed a length of  $L_m$  to enhance efficiency.

The next phase involves expanding the rectangular box originating from  $P_i$ . It is extended in four directions, radiating from point  $P_i$ , as visually depicted in Fig. 4. The expansion step sizes are determined by the variable  $box$ . The initial step size is denoted as  $\tau$ , and each expansion direction may undergo two stages:

- **rapid growth:** The step size  $box_j$  undergoes rapid increments in each iteration, scaling by a factor of  $\gamma$ . If the expansion encounters an obstacle or exceeds  $L_m$ , the step size  $box_j$  is adjusted to the minimum value between  $box_j/4$  and  $\chi$  (refer to Fig. 5a).
- **linear growth:** In this stage, the step size  $box_j$  is maintained at its existing value until an obstacle is encountered. Expansion in the ongoing direction ceases upon collision with an obstacle or when the expansion length reaches  $L_m$  (refer to Fig. 5b).

### D. Dynamic Obstacle Avoidance

The algorithm we propose for online trajectory planning and dynamic obstacle avoidance is presented in Algorithm 4. Our algorithm assumes that the trajectories of dynamic obstacles  $O_{\text{dyn}}$  can be accurately predicted within a short predictive time domain  $T_{\text{pre}}$  using algorithms like those mentioned in [35]–[39]. Here are the specific details of our algorithm:

- 1) **Global Path Planning:** We begin by conducting global path planning using the MVG algorithm to acquire a set of global path points. At this stage, we focus solely on static obstacles and do not account for dynamic obstacles.
- 2) **Local Trajectory Planning:** In this stage, we focus on local trajectory planning. Involves selecting a temporary planning target point, denoted as  $P_{\text{tmp}}$ , based on the planning distance  $D_{\text{plan}}$ . We then use  $P_{\text{tmp}}$  in conjunction with the current AGV position  $P_{\text{cur}}$  to establish a localized planning map known as the  $M_{\text{Local}}$ . All subsequent local trajectory planning activities take place within this map.
- 3) **Dynamic Obstacle Handling:** Within the boundaries of  $M_{\text{Local}}$ , dynamic obstacles, denoted as  $O_{\text{dyn}}$ , are detected, and their trajectories are predicted within the predictive time domain  $T_{\text{pre}}$ . These trajectories are subsequently mapped onto the local map and processed using the approach outlined in Algorithm 1 to obtain

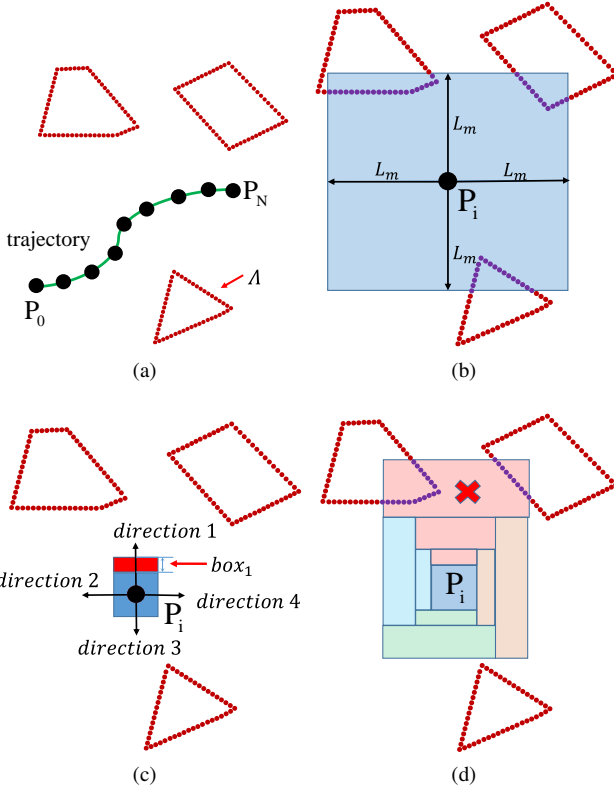


Fig. 4: The creation process of FSRC. (a) path points and obstacle set  $\Lambda$ , (b) initial bounding box  $\mathcal{B}_{\mathcal{R}i}$ , (c) expansion in four directions, (d) expansion encountering obstacles.

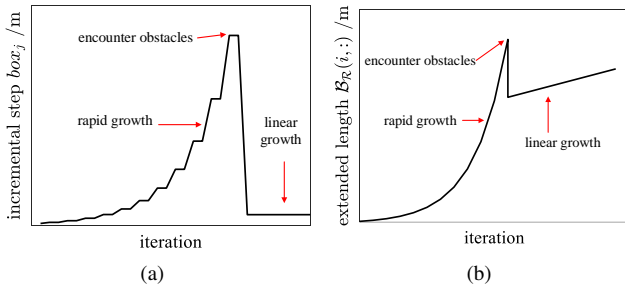


Fig. 5: The two stages of expansion.

an expanded and discrete set of points, denoted as  $\Lambda_{\text{dyn}}$ , representing the dynamic obstacles.

- 4) **Continuation of Trajectory Planning:** Following this dynamic obstacle processing step, the subsequent stages follow the same trajectory planning framework described earlier. We employ the MVG algorithm to generate a set of discrete path points, establish a safe rectangular corridor using the FSRC, and ultimately solve the optimization Problem (1) outlined in the OCP formulation.
- 5) **Task Completion:** The trajectory planning task is considered complete when the current position  $P_{\text{cur}}$  reaches the target point  $g$ .

---

### Algorithm 3 Fast Safe Rectangular Corridor (FSRC)

---

**Require:** path points  $path$ ,  $\Lambda$ ,  $N$

```

1: Initialize parameter  $\tau, \gamma, L_m, \chi$  and  $T_m$ 
2: Initialize a matrix  $\mathcal{B}_{\mathcal{R}}$  of size  $N \times 4$ .
3: for  $i \leftarrow 1$  to  $N$  do
4:    $k \leftarrow 1, x_i \leftarrow X(i), y_i \leftarrow Y(i)$ 
5:   if  $i > 1$  and  $k \leq T_m$  and  $(x_i, y_i)$  in  $\mathcal{B}_{\mathcal{R}}(i-1, :)$ 
   then
6:      $\mathcal{B}_{\mathcal{R}}(i, :) \leftarrow \mathcal{B}_{\mathcal{R}}(i-1, :), k \leftarrow k + 1$ 
7:     continue
8:    $k \leftarrow 1$ 
9:    $\mathcal{B}_{\mathcal{R}}(i, :) \leftarrow [L_m, L_m, L_m, L_m]$ 
10:   $\Lambda_{rm} \leftarrow \text{obsCheck}(\mathcal{B}_{\mathcal{R}}(i, :), \Lambda, x_i, y_i)$ 
11:  if  $\Lambda_{rm} = \emptyset$  then
12:    continue
13:   $\mathcal{U} \leftarrow [0, 0, 0, 0], box \leftarrow [\tau, \tau, \tau, \tau]$ 
14:   $\mathcal{B}_{\mathcal{R}}(i, :) \leftarrow [0, 0, 0, 0]$ 
15:  while  $\text{sum}(\mathcal{U}) < 4$  do
16:    for  $j \leftarrow 1$  to  $4$  do
17:      if  $\mathcal{U}_j = 1$  then
18:        continue
19:       $tmp \leftarrow \mathcal{B}_{\mathcal{R}}(i, :), tmp_j \leftarrow tmp_j + box_j$ 
20:      if  $tmp_j > L_m$  then
21:         $\mathcal{U}_j \leftarrow 1, \text{continue}$ 
22:       $\Lambda_{rm} \leftarrow \text{obsCheck}(\mathcal{B}_{\mathcal{R}}(i, :), \Lambda_{rm}, x_i, y_i)$ 
23:      if  $\Lambda_{rm} = \emptyset$  then
24:         $\mathcal{B}_{\mathcal{R}}(i, :) \leftarrow tmp, box_j \leftarrow box_j \times \gamma$ 
25:      else
26:         $flag \leftarrow 1, box_j \leftarrow \min(box_j / 4, \chi)$ 
27:         $tmp \leftarrow \mathcal{B}_{\mathcal{R}}(i, :) + box_j$ 
28:        while  $flag$  and  $tmp_j < L_m$  do
29:           $\Lambda_{rm} \leftarrow \text{obsCheck}(\mathcal{B}_{\mathcal{R}}(i, :), \Lambda_{rm})$ 
30:          if  $\Lambda_{rm} = \emptyset$  then
31:             $\mathcal{B}_{\mathcal{R}}(i, :) \leftarrow tmp$ 
32:             $tmp_j \leftarrow tmp_j + box_j$ 
33:          else
34:             $flag \leftarrow 0$ 
35:         $\mathcal{U}_j \leftarrow 1$ 
36: return  $\mathcal{B}_{\mathcal{R}}$ 

```

---

## IV. EXPERIMENT

This section focuses on two key aspects: simulation experiments and physical experiments. In the domain of simulation experiments, we conduct a thorough comparative analysis, where we compare our proposed framework against state-of-the-art trajectory planning frameworks to validate its exceptional performance. Subsequently, we evaluate the computational efficiency of our FSRC algorithm against other safe convex corridor-based methods, effectively demonstrating the computational prowess of our approach. Additionally, we present a dynamic obstacle avoidance simulation scenario to illustrate the effectiveness of Algorithm 4.

Shifting our focus to physical experiments, we validate the practical viability of our algorithm through experimentation on a physical platform. The detailed parameter configurations

**Algorithm 4** Online Path Planning and Dynamic Obstacle Avoidance

**Require:** start point  $s$ , goal point  $g$ , static obstacle  $O_{\text{sta}}$ , dynamic obstacles  $O_{\text{dyn}}$ , planning distance  $D_{\text{plan}}$ , predictive time domain  $T_{\text{pre}}$

- 1:  $\text{path} \leftarrow \text{MVG}(s, g, O_{\text{sta}})$   $\triangleright$  global path planning
- 2: **while** Not reached the goal point  $g$  **do**
- 3:  $P_{\text{tmp}} \leftarrow \text{TempTarget}(\text{path}, D_{\text{plan}})$
- 4:  $M_{\text{Local}} \leftarrow \text{DeterminePlanningLocalMap}(P_{\text{tmp}}, P_{\text{cur}})$
- 5:  $\text{DynamicObstacleDetection}(M_{\text{Local}})$
- 6:  $O_{\text{dyn}} \leftarrow \text{PredictDynamicObstaclesTrajectory}(T_{\text{pre}})$
- 7:  $\Lambda_{\text{dyn}} \leftarrow \text{ObtainDynamicObstaclesFootprints}(O_{\text{dyn}})$
- 8:  $\text{path}_l \leftarrow \text{MVG}(P_{\text{cur}}, P_{\text{tmp}}, O_{\text{dyn}}, O_{\text{sta}})$   $\triangleright$  local path planning
- 9:  $\mathcal{B}_{\mathcal{R}} \leftarrow \text{FSRC}(\text{path}_l, \Lambda_{\text{sta}}, \Lambda_{\text{dyn}})$   $\triangleright$  using algorithm 3
- 10:  $\mathfrak{X} \leftarrow \text{SolveOptimizationProblem (1)}$
- 11: Track the trajectory  $\mathfrak{X}$

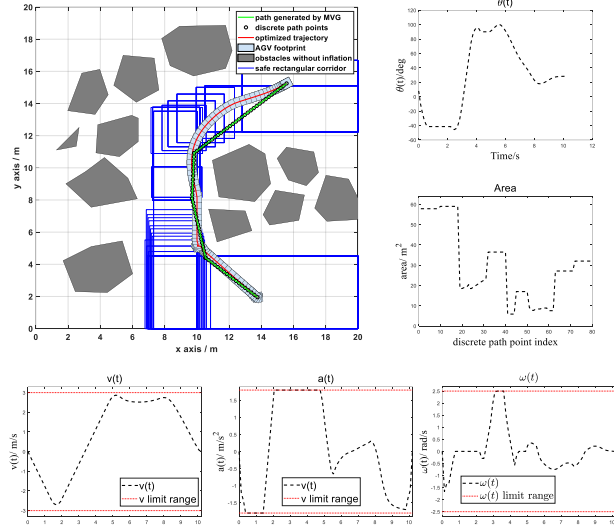


Fig. 6: In a low-density obstacle environment (12 obstacles, Case 1), the simulation results encompass trajectory plots and the temporal evolution of state and control variables, all of which fall within the predefined range. Additionally, the area figure illustrates the area of each rectangular box  $\mathcal{B}_{\mathcal{R}i}$  generated by FSRC.

for both simulation and physical experiments can be found in Table I.

#### A. Simulation

In our simulation experiments, we utilized IPOPT [40] and MA57 [41] as the solvers for the Problem (1). These experiments were carried out using MATLAB 2020b on a desktop computer equipped with an AMD Ryzen 5 3600X 6 Core CPU running at 3.8 GHz and 16 GB of RAM.

Our trajectory planning framework comprises several essential stages, namely polygon obstacle handling (Algorithm 1), path planning based on MVG (Algorithm 2), and the establishment of safe corridors using FSRC (Algorithm 3).

TABLE I: Parameters of the experiment.

Parameter	Value
AGV Length	0.612m
AGV Width	0.582m
maximum speed $v^{\max}$	3.0m/s
maximum acceleration $a^{\max}$	1.8m/s <sup>2</sup>
maximum angular velocity $\omega^{\max}$	2.5rad/s
map size	20m $\times$ 20m
number of discrete points $N$ for Problem (1)	80
discretization precision of obstacle points $\ell$	0.1m
half-length of initial box $L_m$	10m
maximum repetition count $T_m$	8
growth factor $\gamma$	2
minimum growth length $\chi$	0.2m
grid map precision ( $x, y, \theta$ ) for hybrid A*	0.1m, 0.1m, 0.1rad

TABLE II: Efficiency comparison of trajectory planning frameworks (Time: seconds). **Mapping** is map construction time. Our framework uses an adjacency list; others use grid maps. **Path** is path planning time; we use MVG, while others use hybrid A\*. **Corridor** is safe corridor construction time.

case	Method	Mapping	Path	Corridor	Optimization	Total
Case1	Proposed	<b>0.143</b>	<b>0.004</b>	<b>0.103</b>	<b>0.416</b>	<b>0.667</b>
	Area-based	0.387	11.531	-	21.560	33.477
	STC	0.387	11.531	0.473	1.632	14.021
Case2	Proposed	<b>0.285</b>	<b>0.004</b>	<b>0.075</b>	<b>0.375</b>	<b>0.739</b>
	Area-based	0.303	0.276	-	48.055	48.634
	STC	0.303	0.276	0.440	0.811	1.830
Case3	Proposed	<b>0.551</b>	<b>0.004</b>	<b>0.112</b>	<b>0.380</b>	<b>1.049</b>
	Area-based	0.354	28.093	-	5.571	34.018
	STC	0.354	28.093	0.651	0.861	29.605

These stages collectively contribute to the resolution of Problem (1), which is the core trajectory planning problem we aim to solve.

The simulation results of our proposed framework have been presented in three distinct scenarios, as illustrated in Fig. 6 and Fig. 7.. In all three cases, our trajectory planning framework adeptly navigated around obstacles, ensuring safe obstacle avoidance. Specifically, Fig. 6 illustrates that the AGV's speed, acceleration, and angular velocity remained within predefined ranges.

Furthermore, our proposed framework was comprehensively evaluated by comparing it with two state-of-the-art frameworks: the area-based method [42] and STC-based method [26]. It's noteworthy that both of these frameworks employ the hybrid A\* algorithm for initial solutions, which includes the construction of grid maps as an integral part of their processes. The computational times for these three algorithms were summarized in Table II. Significantly, our proposed algorithm outperforms the others in multi-

TABLE III: Efficiency comparison of Safe Convex Corridor-based methods (Time: seconds)

Method	Scenario 1	Scenario 2	Scenario 3	Scenario 4	Mean
FSRC	<b>0.0971</b>	<b>0.0959</b>	<b>0.0825</b>	<b>0.0855</b>	<b>0.0903</b>
STC	0.5766	1.399	0.5034	0.5014	0.7451
SFC	0.2193	0.2288	0.2910	0.2109	0.2375

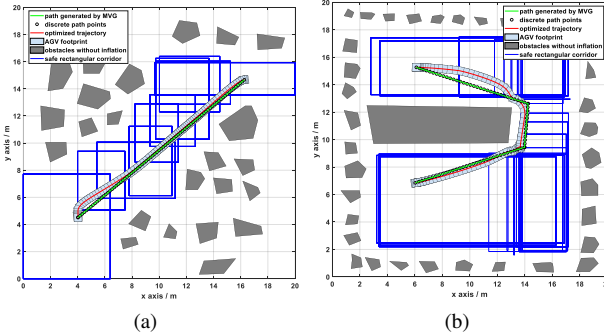


Fig. 7: Simulation results for environments with medium obstacle density (24 obstacles, Case 2) and high obstacle density (36 obstacles, Case 3).

ple aspects, including path planning, optimization problem-solving, and total computation time, highlighting the superior performance of our approach. Moreover, we compared our proposed FSRC algorithm with two other state-of-the-art safe convex corridor-based methods, namely STC [26] and SFC [26]. Our corridor construction efficiency surpasses the other two algorithms, as shown in Table III.

Finally, an application example of Algorithm 4 is presented, as depicted in Fig. 8. The red portions represent the footprints of dynamic obstacles detected by the AGV within a very short planning time, demonstrating the AGV's successful and safe obstacle avoidance.

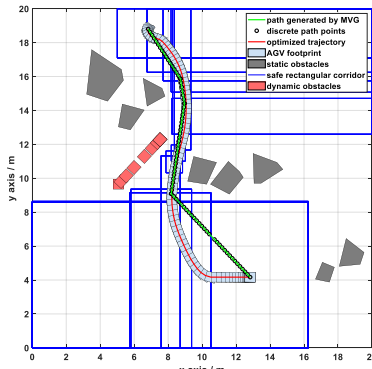


Fig. 8: Experiments on avoiding dynamic obstacles involve planning that only detects a segment of the trajectory of dynamic obstacles.

## B. PHYSICAL EXPERIMENT

Our physical experiment AGV platform is built upon the AgileX SCOUT MINI robot chassis development platform

(refer to Fig. 9). This platform offers exceptional terrain adaptability and ground clearance, enabling agile movement across various surfaces. The fundamental parameters of the SCOUT MINI can be found in Table I. To ensure safety during physical experiments, maximum limits have been imposed: the linear velocity  $v^{\max}$  is set at 1 m/s, and the angular velocity  $\omega^{\max}$  is capped at 1 rad/s. The AGV platform is equipped with a Hokuyo 2D lidar, boasting a maximum range of 30 m, a 9-axis IMU, and an NVIDIA Jetson NX. The NVIDIA Jetson NX features a GPU with 384 cores (Volta architecture @1100MHz + 48 Tensor Cores) and a CPU with NVIDIA Carmel ARMv8.2 (6-core) @1.4GHz (6MB L2 + 4MB L3 cache).

The physical experiment took place within a  $4\text{m} \times 8\text{m}$  environment, where obstacles were strategically arranged using cardboard boxes. The experiment's results can be referenced in Fig. 9.

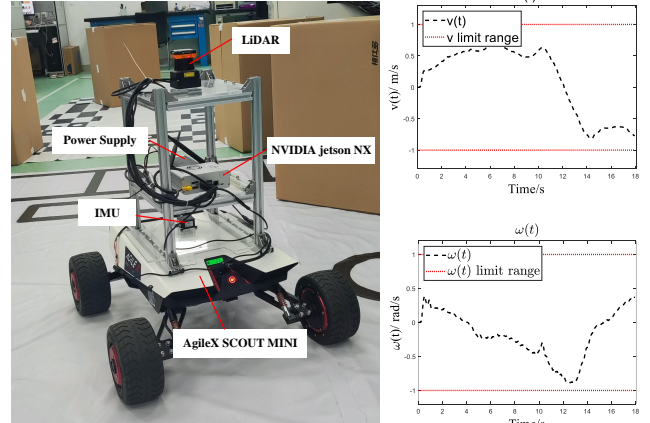


Fig. 9: Physical experiment environment with AgileX SCOUT MINI platform. Additionally, SCOUT MINI exhibits specific linear and angular velocities during navigation.

## V. CONCLUSIONS

This paper presents a practical online fast trajectory planning framework for AGVs in obstacle-rich environments. The trajectory planning problem is formulated as an optimal control problem. Initially, the proposed Modified Visibility Graph is employed for rapid path planning and deriving path points. Subsequently, the proposed Fast Safe Rectangular Corridor algorithm is utilized to quickly establish safe corridors, constraining AGV's path points within corresponding rectangular boxes for optimization. This conversion effectively transforms large-scale non-convex redundant obstacle avoidance constraints into linear and easily solvable box constraints. The effectiveness and superiority of our proposed approach have been validated in both simulation and real-world experiments. Our Fast Safe Rectangular Corridor algorithm significantly improves computation speed compared to state-of-the-art safe convex corridor-based methods. Moreover, our entire trajectory framework performs better than other advanced frameworks.

## REFERENCES

[1] K. Saleh, M. Hossny, and S. Nahavandi, "Real-time intent prediction of pedestrians for autonomous ground vehicles via spatio-temporal densenet," in *2019 International Conference on Robotics and Automation (ICRA)*. IEEE, 2019, pp. 9704–9710.

[2] B. Li, Y. Zhang, Y. Ouyang, Y. Liu, X. Zhong, H. Cen, and Q. Kong, "Real-time trajectory planning for agv in the presence of moving obstacles: A first-search-then-optimization approach," *arXiv preprint arXiv:1902.06201*, 2019.

[3] J. M. Roberts, E. S. Duff, and P. I. Corke, "Reactive navigation and opportunistic localization for autonomous underground mining vehicles," *Information Sciences*, vol. 145, no. 1-2, pp. 127–146, 2002.

[4] X. Zhang, C. Shu, S. Li, C. Wu, and Z. Liu, "Agvs: A new change detection dataset for airport ground video surveillance," *IEEE Transactions on Intelligent Transportation Systems*, vol. 23, no. 11, pp. 20 588–20 600, 2022.

[5] L. Li, Y.-H. Liu, M. Fang, Z. Zheng, and H. Tang, "Vision-based intelligent forklift automatic guided vehicle (agv)," in *2015 IEEE International Conference on Automation Science and Engineering (CASE)*. IEEE, 2015, pp. 264–265.

[6] F. Pratissoli, N. Battilani, C. Fantuzzi, and L. Sabattini, "Hierarchical and flexible traffic management of multi-agv systems applied to industrial environments," in *2021 IEEE International Conference on Robotics and Automation (ICRA)*. IEEE, 2021, pp. 10 009–10 015.

[7] W.-Q. Zou, Q.-K. Pan, and M. F. Tasgetiren, "An effective iterated greedy algorithm for solving a multi-compartment agv scheduling problem in a matrix manufacturing workshop," *Applied Soft Computing*, vol. 99, p. 106945, 2021.

[8] M. Elsisi and M.-Q. Tran, "Development of an iot architecture based on a deep neural network against cyber attacks for automated guided vehicles," *Sensors*, vol. 21, no. 24, p. 8467, 2021.

[9] D. Bechtis, N. Tsolakis, D. Vlachos, and E. Iakovou, "Sustainable supply chain management in the digitalisation era: The impact of automated guided vehicles," *Journal of Cleaner Production*, vol. 142, pp. 3970–3984, 2017.

[10] I. P. Vlachos, R. M. Pascazzi, G. Zobolas, P. Repoussis, and M. Giannakis, "Lean manufacturing systems in the area of industry 4.0: A lean automation plan of agvs/iot integration," *Production planning & control*, vol. 34, no. 4, pp. 345–358, 2023.

[11] B. Farooq, J. Bao, H. Raza, Y. Sun, and Q. Ma, "Flow-shop path planning for multi-automated guided vehicles in intelligent textile spinning cyber-physical production systems dynamic environment," *Journal of manufacturing systems*, vol. 59, pp. 98–116, 2021.

[12] T. Mercy, R. Van Parys, and G. Pipeleers, "Spline-based motion planning for autonomous guided vehicles in a dynamic environment," *IEEE Transactions on Control Systems Technology*, vol. 26, no. 6, pp. 2182–2189, 2017.

[13] F. Yao, B. Alkan, B. Ahmad, and R. Harrison, "Improving just-in-time delivery performance of iot-enabled flexible manufacturing systems with agv based material transportation," *Sensors*, vol. 20, no. 21, p. 6333, 2020.

[14] S. M. LaValle and J. J. Kuffner Jr, "Randomized kinodynamic planning," *The international journal of robotics research*, vol. 20, no. 5, pp. 378–400, 2001.

[15] I. Noreen, A. Khan, and Z. Habib, "Optimal path planning using rrt\* based approaches: a survey and future directions," *International Journal of Advanced Computer Science and Applications*, vol. 7, no. 11, 2016.

[16] P. E. Hart, N. J. Nilsson, and B. Raphael, "A formal basis for the heuristic determination of minimum cost paths," *IEEE transactions on Systems Science and Cybernetics*, vol. 4, no. 2, pp. 100–107, 1968.

[17] M. Buehler, K. Iagnemma, and S. Singh, "Junior: the stanford entry in the urban challenge," *The DARPA urban challenge: autonomous vehicles in city traffic*, vol. 56, pp. 91–123, 2009.

[18] M. Pivtoraiko, R. A. Knepper, and A. Kelly, "Differentially constrained mobile robot motion planning in state lattices," *Journal of Field Robotics*, vol. 26, no. 3, pp. 308–333, 2009.

[19] M. Pivtoraiko and A. Kelly, "Efficient constrained path planning via search in state lattices," in *International Symposium on Artificial Intelligence, Robotics, and Automation in Space*. Munich Germany, 2005, pp. 1–7.

[20] A. I. Panov, K. S. Yakovlev, and R. Suvorov, "Grid path planning with deep reinforcement learning: Preliminary results," *Procedia computer science*, vol. 123, pp. 347–353, 2018.

[21] X. Lei, Z. Zhang, and P. Dong, "Dynamic path planning of unknown environment based on deep reinforcement learning," *Journal of Robotics*, vol. 2018, 2018.

[22] J. Xin, H. Zhao, D. Liu, and M. Li, "Application of deep reinforcement learning in mobile robot path planning," in *2017 Chinese Automation Congress (CAC)*. IEEE, 2017, pp. 7112–7116.

[23] B. Li, Y. Zhang, Y. Ouyang, Y. Liu, X. Zhong, H. Cen, and Q. Kong, "Fast trajectory planning for agv in the presence of moving obstacles: A combination of 3-dim a\* search and qcqp," in *2021 33rd Chinese Control and Decision Conference (CCDC)*. IEEE, 2021, pp. 7549–7554.

[24] B. Li, K. Wang, and Z. Shao, "Time-optimal maneuver planning in automatic parallel parking using a simultaneous dynamic optimization approach," *IEEE Transactions on Intelligent Transportation Systems*, vol. 17, no. 11, pp. 3263–3274, 2016.

[25] S. Shi, Y. Xiong, J. Chen, and C. Xiong, "A bilevel optimal motion planning (bomp) model with application to autonomous parking," *International Journal of Intelligent Robotics and Applications*, vol. 3, no. 4, pp. 370–382, 2019.

[26] B. Li, T. Acarman, X. Peng, Y. Zhang, X. Bian, and Q. Kong, "Maneuver planning for automatic parking with safe travel corridors: A numerical optimal control approach," in *2020 European Control Conference (ECC)*. IEEE, 2020, pp. 1993–1998.

[27] Y. Li, S. Liang, J. Gao, Z. Chen, S. Qiao, and Z. Yin, "Trajectory optimization for the nonholonomic space rover in cluttered environments using safe convex corridors," *Aerospace*, vol. 10, no. 8, p. 705, 2023.

[28] J. Lian, W. Ren, D. Yang, L. Li, and F. Yu, "Trajectory planning for autonomous valet parking in narrow environments with enhanced hybrid a\* search and nonlinear optimization," *IEEE Transactions on Intelligent Vehicles*, 2023.

[29] Z. Zhu, E. Schmerling, and M. Pavone, "A convex optimization approach to smooth trajectories for motion planning with car-like robots," in *2015 54th IEEE conference on decision and control (CDC)*. IEEE, 2015, pp. 835–842.

[30] S. Liu, M. Watterson, K. Mohta, K. Sun, S. Bhattacharya, C. J. Taylor, and V. Kumar, "Planning dynamically feasible trajectories for quadrotors using safe flight corridors in 3-d complex environments," *IEEE Robotics and Automation Letters*, vol. 2, no. 3, pp. 1688–1695, 2017.

[31] B. Li, Z. Yin, Y. Ouyang, Y. Zhang, X. Zhong, and S. Tang, "Online trajectory replanning for sudden environmental changes during automated parking: A parallel stitching method," *IEEE Transactions on Intelligent Vehicles*, vol. 7, no. 3, pp. 748–757, 2022.

[32] J. H. Mathews, K. D. Fink *et al.*, *Numerical methods using MATLAB*. Pearson prentice hall Upper Saddle River, NJ, 2004, vol. 4.

[33] T. Lozano-Pérez and M. A. Wesley, "An algorithm for planning collision-free paths among polyhedral obstacles," *Communications of the ACM*, vol. 22, no. 10, pp. 560–570, 1979.

[34] E. W. Dijkstra, "A note on two problems in connexion with graphs," in *Edsger Wybe Dijkstra: His Life, Work, and Legacy*, 2022, pp. 287–290.

[35] K. Min, D. Kim, J. Park, and K. Huh, "Rnn-based path prediction of obstacle vehicles with deep ensemble," *IEEE Transactions on Vehicular Technology*, vol. 68, no. 10, pp. 10 252–10 256, 2019.

[36] X. Song, K. Chen, X. Li, J. Sun, B. Hou, Y. Cui, B. Zhang, G. Xiong, and Z. Wang, "Pedestrian trajectory prediction based on deep convolutional lstm network," *IEEE Transactions on Intelligent Transportation Systems*, vol. 22, no. 6, pp. 3285–3302, 2020.

[37] H. Zhao, J. Gao, T. Lan, C. Sun, B. Sapp, B. Varadarajan, Y. Shen, Y. Shen, Y. Chai, C. Schmid *et al.*, "Tnt: Target-driven trajectory prediction," in *Conference on Robot Learning*. PMLR, 2021, pp. 895–904.

[38] J. Yue, D. Manocha, and H. Wang, "Human trajectory prediction via neural social physics," in *European Conference on Computer Vision*. Springer, 2022, pp. 376–394.

[39] Y. Yuan, X. Weng, Y. Ou, and K. M. Kitani, "Agentformer: Agent-aware transformers for socio-temporal multi-agent forecasting," in *Proceedings of the IEEE/CVF International Conference on Computer Vision*, 2021, pp. 9813–9823.

[40] A. Wächter and L. T. Biegler, "On the implementation of an interior-point filter line-search algorithm for large-scale nonlinear programming," *Mathematical programming*, vol. 106, pp. 25–57, 2006.

[41] A. HSL, "collection of fortran codes for large-scale scientific computation," *See <http://www.hsl.rl.ac.uk>*, 2007.

[42] B. Li and Z. Shao, "A unified motion planning method for parking an

autonomous vehicle in the presence of irregularly placed obstacles,”  
*Knowledge-Based Systems*, vol. 86, pp. 11–20, 2015.